BMC Chemistry

RESEARCH

Open Access

Use of gold/iron metal-organic framework nanoparticles (AuNPs/FeMOF)-modified glassy carbon electrode as an electrochemical sensor for the quantification of risperidone in patient plasma samples

Zahra Golsanamlu[2†], Haniyeh Pashanejad[3†], Elaheh Rahimpour[1], Abolghasem Jouyban[1], Afsaneh Farjami[3], Jafar Soleymani[1*] and Fatemeh Ranjbar[4]

Abstract

Risperidone (RIS) is one of the most prescribed atypical antipsychotics approved for the treatment of various neuropsychiatric diseases. For the correlation of serum concentration and pharmacological effects of RIS, therapeutic drug monitoring is considered a fundamental concept for clinical application. This paper is provided to develop an electrochemical probe for the determination of RIS in biological samples by modification of glassy carbon electrode (GCE) using gold nanoparticles (AuNPs) and iron metal-organic-frameworks (FeMOFs). This probe fabrication process was characterized with various techniques including Fourier transform infrared (FTIR), emission scanning electron microscopy (FESEM), energy dispersive X-ray (EDX), atomic force microscopy (AFM), and dynamic light scattering (DLS) to confirm the proper synthesis of materials and the sensors designing. The developed probe square-wave voltammetry (SWV) signal was linear upon RIS concentration from 0.02 to 50 µg/mL with a low limit of quantification (LOQ) of 0.02 µg/mL. Based on the validated method, high accuracy and precision, good specificity, and suitable stability of fabricated probes were achieved. As the ultimate step, this method was successfully applied for the quantification of RIS in patients' plasma samples with regular RIS consumption. The fabricated electrochemical demonstrates favorable clinical applicability due to its simplicity, high sensitivity, low sample pretreatment time, and rapid analysis time, making it a promising probe as an alternative to current separation-based methods. Also, the developed probe is cost-effective, as it uses a low amount of materials, decreases sample processing time, and utilizes inexpensive materials, which could remarkably reduce the overall cost of RIS concentration detection in clinical samples. The obtained results showed the potential of the developed probe for fast and reliable detection of RIS in plasma samples.

†Zahra Golsanamlu and Haniyeh Pashanejad contributed equally to this work.

*Correspondence:
Jafar Soleymani
jsoleymanii@gmail.com; soleymanij@tbzmed.ac.ir

Full list of author information is available at the end of the article

Keywords Electrochemical detection, Risperidone, Biomedical analysis, Unprocessed plasma

Introduction

Neuropsychiatric diseases are usually accompanied by patients lifelong which bring those disabilities and heavy economic burden. Since 1950s, antipsychotics were introduced as neuroleptics use in clinical psychiatry, atypical antipsychotics have been reached the top-sell categories of pharmaceuticals [1, 2]. Atypical antipsychotics (second generation antipsychotics) antagonized both dopaminergic and serotonin (5HT2) receptors in brain which reduced propensity to cause extrapyramidal adverse effects [3]. Risperidone (RIS) with a molecular formula of $C_{23}H_{27}FN_4O_2$ is one of the most used atypical antipsychotics approved for treatment of schizophrenia, short-term manic states of bipolar disorder, autism, and attention-deficit disorders [4, 5]. Additionally, off-label uses of RIS include obsessive-compulsive disorder, disruptive behavior disorders, treatment-resistant depression, tourette syndrome, etc [6–8]. According to clinical guidelines, recommended serum therapeutic reference for RIS is ranged from 20 to 60 ng/mL combined of RIS and 9-hydroxyrisperidone (an active metabolite with similar pharmacological activity) serum concentration. Moreover, RIS is most evidence-supported atypical antipsychotic indicates direct correlation of serum concentration and pharmacological effects and levels above 120 ng/mL are associated with the adverse effects like development of parkinsonian symptoms and hyperprolactinemia [8]. So, therapeutic drug monitoring (TDM) considered as a true-of-certain concept that reflect the regulation of efficacy and incidence of severe side effects in patients with RIS therapeutic regimen [9].

Previous studies for the quantification of RIS mostly have been concerned with high performance liquid chromatographic-ultraviolet (HPLC-UV) detector [10–12], electrochemical detection [13], and mass spectrometry (MS) [9, 14–18]. Although these methods provide great sensitivity and selectivity, the high-cost instrumentation, require time-consuming extraction processes, need of specialized technicians and long run-times made them not conducive to clinical promotion [8, 19, 20]. To provide sustained monitoring technique of RIS, a constant need for the development of simple, fast, sensitive and miniaturized automation method have been comprehended in recent years.

Electrochemical methods possess a multitude of advantages like rapid analysis, cost-effectiveness and high sensitivity which made them a as a promising technique for point-of-care applications [21, 22]. The desired substrate in electrochemical sensors should have some essential properties such as high electrical conductivity, extensive surface area, stable background current, good corrosion resistance, and efficient chemical and electrical stabilities [23]. Due to the significant advancement in nanotechnology, the modification of the surface of electrodes has resulted in enhancement the performance of current electrochemical sensors and provide higher sensitivity and precision in analytical determinations [8, 23]. For instance, Merli et al. reported modification of a gold electrode by oxidized carbon nanotubes for the RIS determination in urine samples [24]. In another study, Arvand et al. utilized multi-walled carbon nanotube modified glassy carbon electrode (GCE) for RIS detection in biological fluids [4]. Shahrokhian et al. employed various modified electrodes functionalized by carbon nanoparticles, carbon nanotubes (CNTs), nanodiamond/graphite, and reduced graphene oxide on GCE [23].

Applications of new materials enhanced the efficiency the developed new sensing platforms and improved their selectivity as well [25, 26]. MOFs are a new model crystalline structures of metal ions and organic ligands comprising proprieties of inherent porosity, numerous metal active sites, high surface-to-volume ratio, good stability, and tunable shape size which made them a multifunctional candidate for sensor designing applications [27–29]. By selecting of different metal ions, several MOFs-based structures were synthetized in an easy manner. It's notable to mention that binding agent in MOFs structure play the crucial role in ability of ions absorption. Combination of Iron (Fe) and MOFs exhibit strong affinity to anions as Cl, Br, P, N and S. Fe is highly abundant and easy obtained element in environment [30].

Gold nanoparticles (AuNPs) are one of the main materials in the preparation of electrochemical sensors for the measurement of various analytes. Also, AuNPs have been employed for preparation of various drug-delivery [31], bioimaging [32, 33], and other biomedical applications. A review of the literature showed that AuNPs are used for the detection of drugs, biomarkers, environmental pollutants, DNA/RNA, etc [34, 35]. This is due to the increased additive properties, increased specific surface area, increased electroanalytical activities, relatively high stability, and high biocompatibility. In this study, AuNPs have been used to optimize the surface of a GCE to increase the analytical performance of the probe. This increase in performance will be achieved by increasing the electron transfer kinetics at the electrode surface by AuNPs. This paper discuss the development an electrochemical assay for the quantification of RIS in biological samples. The proposed method is based on the application of metal-organic frameworks (MOFs) for modification the surface of GCE. The FeMOFs nanoparticles were immobilized on the surface of the GCE, which expressed

significant electrochemical performance towards the RIS in unprocessed plasma samples. Additionally, the modified FeMOF/AuNPs/GCE presents favorable sensitivity, excellent specificity, and promising stability for detecting RIS in patients' samples.

Experimental

Chemicals and reagents

RIS powder was purchased from Sobhan Darou pharmaceutical Co. (Karaj, Iran). Dimethylformamide (DMF), sodium hydroxide (NaOH), hydrochloric acid (HCl), sulfuric acid (H_2SO_4), nitric acid (HNO_3 65%), chloroauric acid ($HAuCl_4$), ethanol, ferric chloride hexahydrate ($FeCl_3.6H_2O$), and benzenedicarboxylic acid (H_2BDC) are purchased from Sigma (Germany). Disodium hydrogen phosphate (Na_2HPO_4) and Sodium dihydrogen phosphate (NaH_2PO_4) were employed to prepare buffer solutions provided from Merck (Darmstadt, Germany). Plasma blank samples have been provided by the Iranian Blood Transfusion Organization (Tabriz, Iran).

Instruments

Fourier transform infrared (FTIR) from Bruker model instrument (Massachusetts, USA) was used to the identification of the functional groups. The structural morphology was characterized by the field emission scanning electron microscopy (FESEM) of (FEG-SEM MIRA3 TESCAN Company (Brno, Czech Republic) Also, the energy dispersive X-ray (EDX) spectra was determined by the same instrument. Atomic force microscopy (AFM) was used to study surface topography through a Digital Instruments nanosurf mobile S (Grammetstrasse, Switzerland). Zeta potential and dynamic light scattering (DLS) were considered by a Malvern particle size analyzer (Malvern, UK). An AUTOLAB electrochemical system using an Ag/AgCl electrode, GCE, and a platinum electrode served as the reference, working, and counter electrodes for recoding the electrochemical voltammograms.

Synthesis

Preparation of FeMOF

The solvothermal method was employed to synthesize of FeMOFs, which already reported by Sintya et al. [36]. Briefly, the mixture of $FeCl_3.6H_2O$ (0.675 g) and H_2BDC (0.206 g) dissolved completely in DMF (30 mL) and heated in a Teflon-lined autoclave and heated at 150 °C for about 24 h. The product was washed by DMF and collected by centrifugation. Finally, black solid dried at 60 °C over night.

Synthesis of AuNPs

AuNPs were synthesized using the citrate reduction method described by Chaichi et al. [37]. 100 mL of boiling $HAuCl_4$ (0.01%) solution and 2 mL of sodium citrate (1%) solution was mixed quickly under vigorous stirring to observe color alteration from colorless to wine-red and then was kept at 4 °C in dark condition for the next uses.

Sensor design

Electrode pretreatment

Before any electrode modification, the GCE electrode was polished using a high-meshed alumina powder. It was then rinsed with water and inserted in acetone for approximately 5 min, and washed with water. Then, the bare electrode was submerged in the solution of H_2SO_4 (0.05 M) and HNO_3 (0.050 M) for 5 min to remove any organic contamination and then washed with distilled water. Ultimately, cyclic voltammetric (CV) technique was run in H_2SO_4 (0.1 M) solution with potential between– 1.2 and 1.2 V for 25 cycles until reach stable CVs.

Electrodeposition of AuNPs and preparing the final probe

A GCE bare electrode was immersed into the solution of AuNPs to electrodeposit using chronoamperometry (ChA) at $E_1 = 0.00$ V for a given time from 1 to 250 s. To the best of our knowledge, ChA was considered as the best electrodeposition mode for controlling the growth of nanoparticles size and film thickness [38]. Subsequently, AuNPs attached on the surface of GCE. For the fabrication of FeMOF/AuNPs/GCE electrode, a proper volume of the dispersed FeMOF (5 µL) was casted on the AuNPs/GCE and dried for 10 min.

Detection approach

After preparing the probe, different standards were prepared by adding appropriate amount of RIS in supporting electrolyte and the corresponding electrochemical signal was recorded. Also, to plot the calibration curve in plasma media, a certain amount of blank plasma has been spiked with various RIS concentrations and centrifuged the mixture (10.000 rpm, 10 min). Next, without performing any additional step, the mixture was added to supporting electrolyte and record the electrochemical signal (Scheme 1).

Results and discussions

Characterization of FeMOF/AuNPs/GCE and FeMOF nanoparticles

Figures 1 and 2 show FESEM images of FeMOF morphology in which their particular octahedral shape [39–41] is observable with size of around 300 nm. This FESEM sizes was confirmed with DLS size analyzer with mean value of 364 nm with a polydispersity index (PdI) of 0.66, showing broad size distribution (Fig. 1S(a)). Moreover, the surface charge of FeMOF was evaluated by zeta

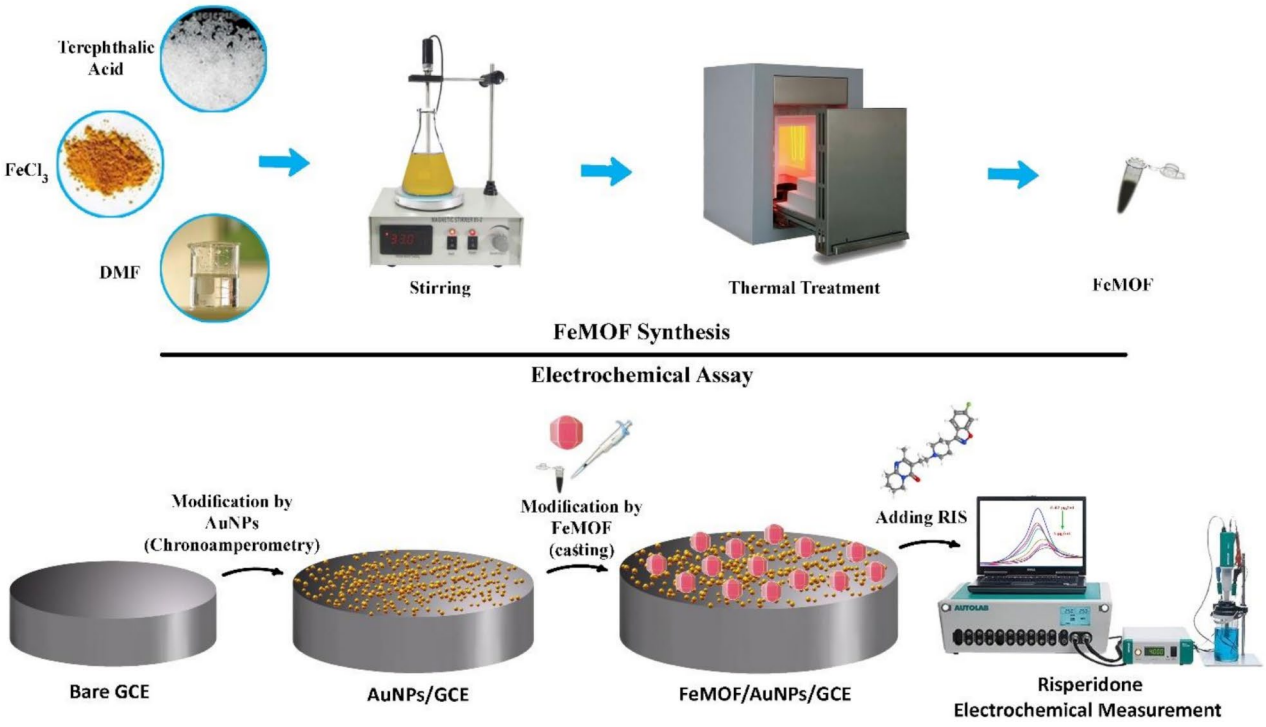

Scheme 1 Schematic demonstration of the FeMOF/AuNPs/GCE-based sensor fabrication and quantification of RIS using electrochemical method

potential analyzer (Fig. 1S(b)) with a positive zeta value of +0.5 mV. Figure 2 shows the roughness and uniformly distribution of FeMOF/AuNPs on GCE surface. In fact, the roughness of the deposited layer can assist the diffusion of analyte through the supporting electrolyte to get closer to the sensing layer. Moreover, the well-combined and well-dispersed AuNPs with FeMOF may covered surface area and make the porous layer with cavities on the electrode surface to allow electrochemically react of RIS molecules upon a dual signal amplification mechanism. Also, AFM analysis of FeMOF/AuNPs/GCE confirmed the topography of the nanoparticles as determined by FE-SEM (Fig. 2S). FeMOF/AuNPs are disposed on the surface vertically and a mean height of around 50 nm was estimated for them.

The functional groups of FeMOF were confirmed by FTIR technique (Fig. 3S). C = O bonds of benzenecarboxylic group were detected at wavenumber of 1607 cm^{-1} and peak around 1400 cm^{-1} is attributed to the C-C vibration in aromatic carbon groups [36]. Hydrogen bond may be affected C = O position to the longer wavenumbers [42]. The stretching and bending vibration of O–Fe–O and Fe–O–Fe are corresponded in around 500–700 cm^{-1} as a signature peak of FeMOF. The bands obtained at 3373 cm^{-1} were attributed the stretching vibrations of the O–H. The elemental composition of the FeMOF/AuNPs/GCE by EDX and map analysis declared the elemental percentages of C, O, Fe and Au are 63.68%, 30.80%, 63.33%, 1.96%, and 3.56%, respectively (Fig. 4S and Table 1S). While, FeMOF consists of C (94.68%), O (1.70%) and Fe (3.62%) and Au peak was not observed in EDX analysis (Fig. 5S and Table 2S).

Electrochemical characterization of FeMOF/AuNPs/GCE

Since RIS is electrochemically inactive and does not have any oxidation/reduction peaks within the potential window, it cannot be measured by direct methods. To overcome this problem and utilize the advantages of electrochemical methods in RIS analysis, an indirect method was chosen by blocking the redox activity of $[Fe(CN)_6]^{-4}$/$[Fe(CN)_6]^{-3}$ by RIS. $[Fe(CN)_6]^{-4}$/$[Fe(CN)_6]^{-3}$ undergoes a reversible one-electron oxidation/reduction reaction at the optimized electrode surface, generating a current. In the presence of RIS and attaching to the electrode surface, the electroactive sites on the electrode surface are blocked by RIS molecules, limiting the transfer of $[Fe(CN)_6]^{-4}$/$[Fe(CN)_6]^{-3}$ to the electrode surface, which reduces the current. The reduced current is proportional to the concentration of RIS, which determines its indirect value.

The choice of conjugated salt as the supporting electrolyte is due to its advantages such as reversible oxidation/reduction reaction kinetics, specific diffusion coefficient for accurate calculation of electrode surface area and other electrochemical parameters using the Randles–Ševčík equation, stable water solution, etc.

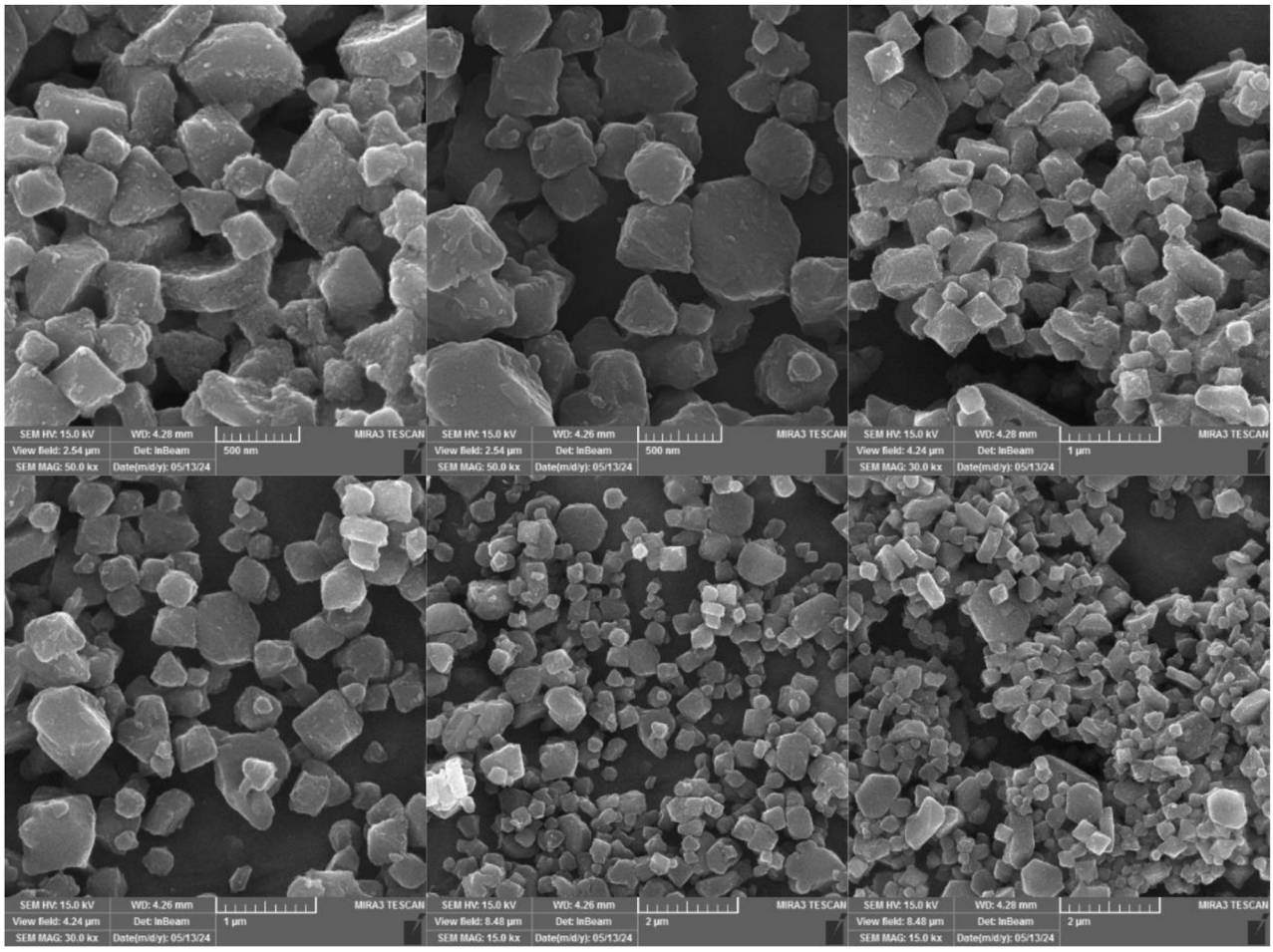

Fig. 1 FESEM images of FeMOF particles with corresponding scale bars at different magnifications

Figure 6S displays the ChA plot of the electrodeposition of the AuNPs onto the surface of GCE (Sect. 2.4.2) in $E_1 = 0.00$ V [34]. The gradually increasing of current intensity during the time progress indicates the surface full electrodeposition of the AuNPs. After about 200 s, the current intensity remained constant, indicating the maximum electrodeposition of AuNPs on the bare GCE surface.

The CV responses of the redox probe was also studied during step-by-step surface modification of GCE with FeMOF and AuNPs along with CVs of the probe in the presence and absence of RIS. Figure 3 demonstrates CVs of bare GCE, and AuNPs/GCE, FeMOF/AuNPs/GCE in the presence and absence of RIS (20 µg/mL) in the supporting electrolyte solution (pH = 5.0, 5 mM of $[Fe(CN)_6]^{-4}/[Fe(CN)_6]^{-3}$) in the potential from −1.0 to +1.0 V and sweep rate of 100 mV/s (from lower to higher potential). The peak current increase beyond the addition of AuNPs and FeMOFs due to the dual amplification mechanism. So, the modification of the GCE surface improves the electrochemical activity compared with bare electrode. The $[Fe(CN)_6]^{-4}/[Fe(CN)_6]^{-3}$ pair potential was changed to 0.29 V, confirming the successful surface modification of the electrode with AuNPs and FeMOFs. Upon adding the RIS, peak current decreased at 0.29 V resulted, leading to the blocking of the redox pair electro-oxidation. The nanoparticles enhance the area-to-volume of the composite to facilitate the redox reaction ($[Fe(CN)_6]^{-4}/[Fe(CN)_6]^{-3}$).

Effect of pH

Standard solution of RIS was utilized for optimization of pH value which strongly influences the electrochemical performance by involving the proton transfer. Figure 7S(a) illustrated the changes of CVs potential and current of the redox pair in different pHs ($2.0 < pH < 10.0$). As the pH was gradually increased, the potential shifted towards more positive values and the current peak decreased. Because the increase in concentration of hydrogen ions is accompanied with increasing in redox potentials [43]. Beyond pH 5.0 a distortion in the peak shapes was observed. Figure 7S(b) shows the

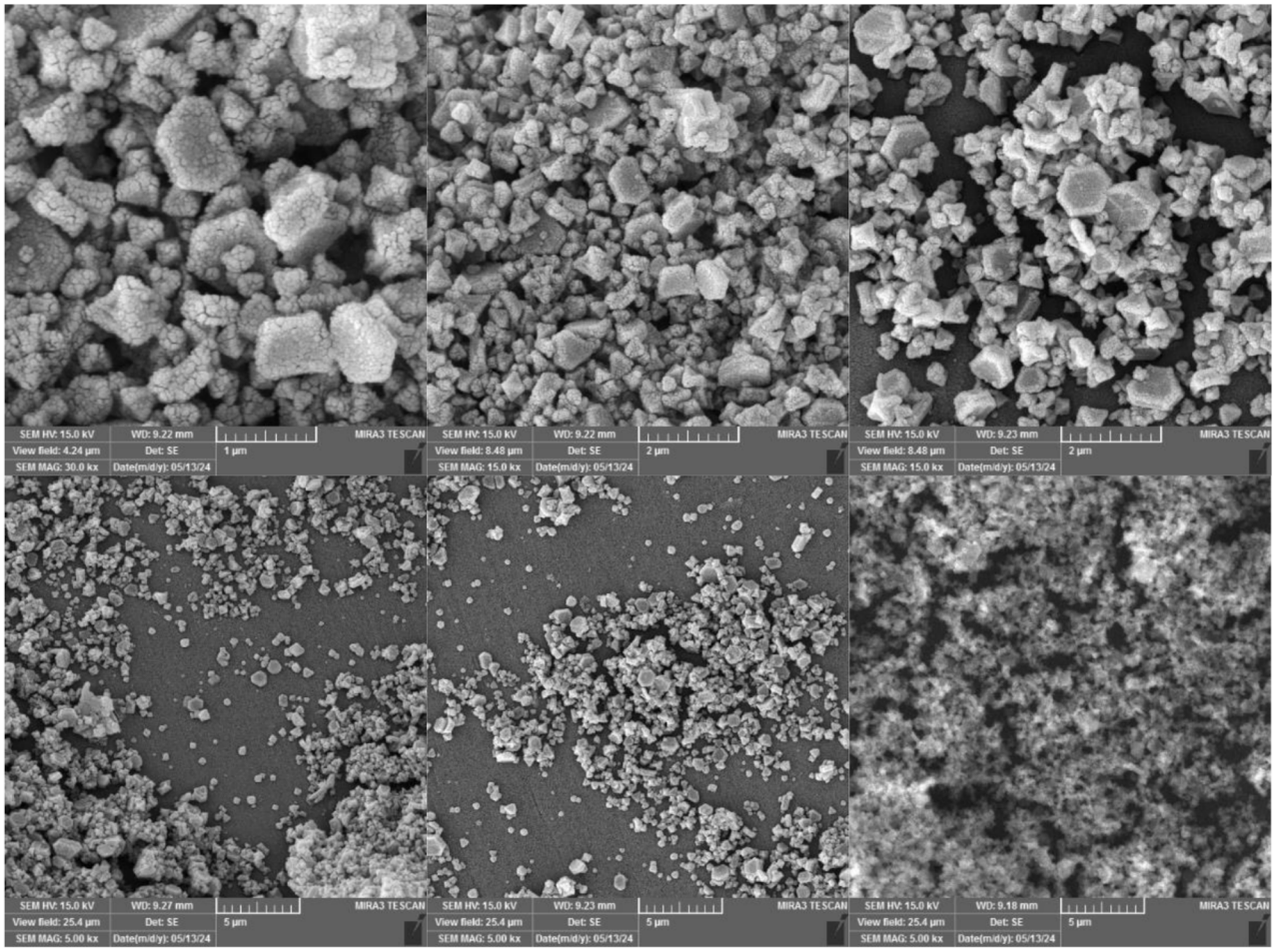

Fig. 2 FESEM images of FeMOF/AuNPs/GCE electrode with corresponding scale bars at different magnifications

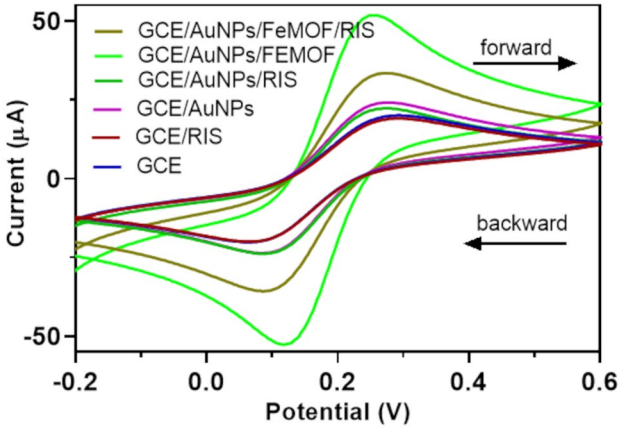

Fig. 3 CVs of bare GCE, AuNPs/GCE, and FeMOF/AuNPs/GCE in the presence and absence of RIS (20 µg/mL). (pH 5.0, $[Fe(CN)_6]^{-4}/[Fe(CN)_6]^{-3}$, 5 mM, KCl 0.1 M, sweep rate 100 mV/s)

linear function of potential of anodic peak over the pH range of 3–10.

$$E_{pa}\,(V) = 0.08314\,\mathrm{pH} - 0.07310,\ R^2 = 0.9749$$

The obtained slope is 0.08314 V/pH which is approximately near to 0.0592 V/pH as the theoretical value, suggesting total number of electrons and the protons that in the presence of RIS are equal.

Kinetic study and estimation of the surface area

Figure 8S (a) displays the CV of successive scan rate of the bare GCE, AuNPs/GCE, and FeMOF/AuNPs/GCE from 2 mV/s to 500 mV/s. To study the kinetic of the electrooxidation, the oxidation peak current ($I_{p.a.}$) and square roots of scan rates ($v^{0.5}$) was firstly plotted. Figure 8S (b) is presenting a linear relationship $I_{p.a.}$ *vis* $v^{0.5}$ with an equation of Ipa (µA) = 2.079 ν0.5(mV/s) + 3.245 (R^2 = 0.9974), Ipa (µA) = 1.326 ν0.5(mV/s) + 5.241 (R^2 = 0.9889), and $I_{p.a.}$ (µA) = 0.5554 $v^{0.5}$(mV/s) + 4.002 (R^2 = 0.9717) for FeMOF/AuNPs/GCE, AuNPs/GCE, and bare GCE, respectively,

proposing the diffusion-controlled electrooxidation of $[Fe(CN)_6]^{3-/4-}$ on the FeMOF/AuNPs modified GCE. Therefore, the Randles–Sevcik equation can be utilized to explain the electrooxidation process on the surface of the FeMOF/AuNPs modified GCE. This equation is as follows.

$$I_{pa} = 2.69 \times 10^5 AD^{0.5} n^{1.5} C v^{0.5}$$

Here, $I_{p.a.}$, D, A, υ, C, and n, denote to anodic peak current (A), the molecular diffusion coefficient of the electrolyte (cm^2/s), electroactive surface area (cm^2), scan rate (mV/s), C (M), and number of electron, respectively.

Also, ln $I_{p.a.}$*vis* ln υ was in the scan rate range with an equation of Ipa (μA) = 0.3684 ln υ (mV/s) + 1.478 (R^2 = 0.9914), Ipa (μA) = 0.3563 ln υ (mV/s) + 1.1.318 (R^2 = 0.9991), and Ipa (μA) = 0.2618 ln υ (mV/s) + 1.084 (R^2 = 0.9987), for FeMOF/AuNPs/GCE, AuNPs/GCE, and bare GCE, respectively (Fig. 8S(c)). As could be seen, the slope is near to the 0.5, proposing diffusional-controlled mass transferring on the surface of the FeMOF/AuNPs modified GCE (Fig. 8S(c)). The non-linear relationship between $I_{p.a.}$*vis* υ was further confirmed the diffusional-controlled mass transferring mechanism on the surface of FeMOF/AuNPs/GCE, AuNPs/GCE, and bare GCE electrodes (Fig. 8S(d)).

The surface area of the modified FeMOF/AuNPs/GCE, AuNPs/GCE, and bare GCE electrodes could be calculated using Randles–Sevcik equation. For this, the slope of $I_{p.a.}$*vis* $υ^{0.5}$ was employed by substituting, n, C, and D of 1, 10 mM, and 0.76×10^{-5} cm^2/s, respectively. The calculated value for the electrodes are as 0.5607 cm^2, 0.3576 cm^2, and 0.1498 cm^2, for FeMOF/AuNPs/GCE, AuNPs/GCE, and bare GCE, respectively. These results proposed that the surface modification of GCE with AuNPs and AuNPs/FeMOF can enhance the signal of the sensor by 2.4 and 3.8 times, showing the proper surface modification and materials selection in the sensor designing process.

Optimization of analytical condition

In general, the electrochemical performance of modified electrode may influence by conditional factors. In the first step, the effect of the electrode composition was examined using different amount of AuNPs and FeMOF which are optimum current intensity was observed by 12.5 mM (Fig. 4(a)) and 2000 μg/mL (Fig. 4(b)), respectively. In fact, by increasing their amount, the thickness of the modifiers provide a porous film covered electrode surface resulting in the enhancement of the amount of active sites for the electrochemical reaction. In higher concentrations, peak current reduced due to the increasing of improper mechanical property which decreased the adherence of the modifier layer [23].

To find the optimum pH, the electrochemical behavior of RIS was studied in different pH values from 2 to 11 *versus* the ratio of the current intensity in the presence and absence of the analyte (Fig. 4(c)). It was found that the voltammetric oxidation of RIS at the surface of electrode was more favorite under acidic conditions of phosphate buffer (50 mM) and it reaches its maximum value at pH 5.0. Furthermore, the effect of buffer concentration is depicted at Fig. 4(d).

Linearity and sensitivity

Under optimized conditions, FeMOF/AuNPs modified GCE was applied for determining of RIS in plasma samples. The gradual increase in RIS concentration (Fig. 5(a)) was found to correspond with a decrease in the peak current intensity. In this study, signal ratio of the probe in the presence and absence of analyte was regarded as analytical signal. The calibration plot was obtained by ratio of peak current (analyte/blank) vs. RIS concentrations with a linear segment of 0.02–5 μg/mL through the regression equation derived as y= -0.06942 log[RIS] + 0.2402 (R^2 = 0.9985) (Fig. 5(b)). Also, the method's low limit of quantification (LLOQ) for RIS was obtained as 0.02 μg/mL.

Table 1 compares the analytical features of modified electrode to previously reported in the literature [4, 8, 19, 44, 45]. Three different techniques have been reported for the measurement of RIS in different samples. In general, electrochemical methods have the advantage of being less expensive and more portable than optical and separation methods, respectively. Also, this method has better sensitivity than other reported electrochemical methods. The developed assay provide an effective internal referencing and self-calibrating system which minimizes the instrument function variation and matrix effects [46]. It is concluded that the developed probe is able to quantify RIS concentrations in a wide range in plasma samples without requiring to any pretreatment steps. While the separation-based and optical methods usually need protein precipitation steps to remove interfering biomolecules led to wash out the amounts of analyte. This type of analytical method can be used as reliable technique in clinical setting, where an extensive number of plasma samples needed to be quantified in a short period [47–49].

Validation section

Precision and accuracy study

The accuracy of an analytical method, expressed as relative error percentage (RE%) was assessed by repeated analysis of three RIS-spiked plasma samples containing known concentrations (0.05-0.5-5.0 μg/mL) for which the inter-day accuracy ranged from −4.4 to 8.9%. Also, the interday and intraday repeatability of the developed method for the same concentrations were calculated by

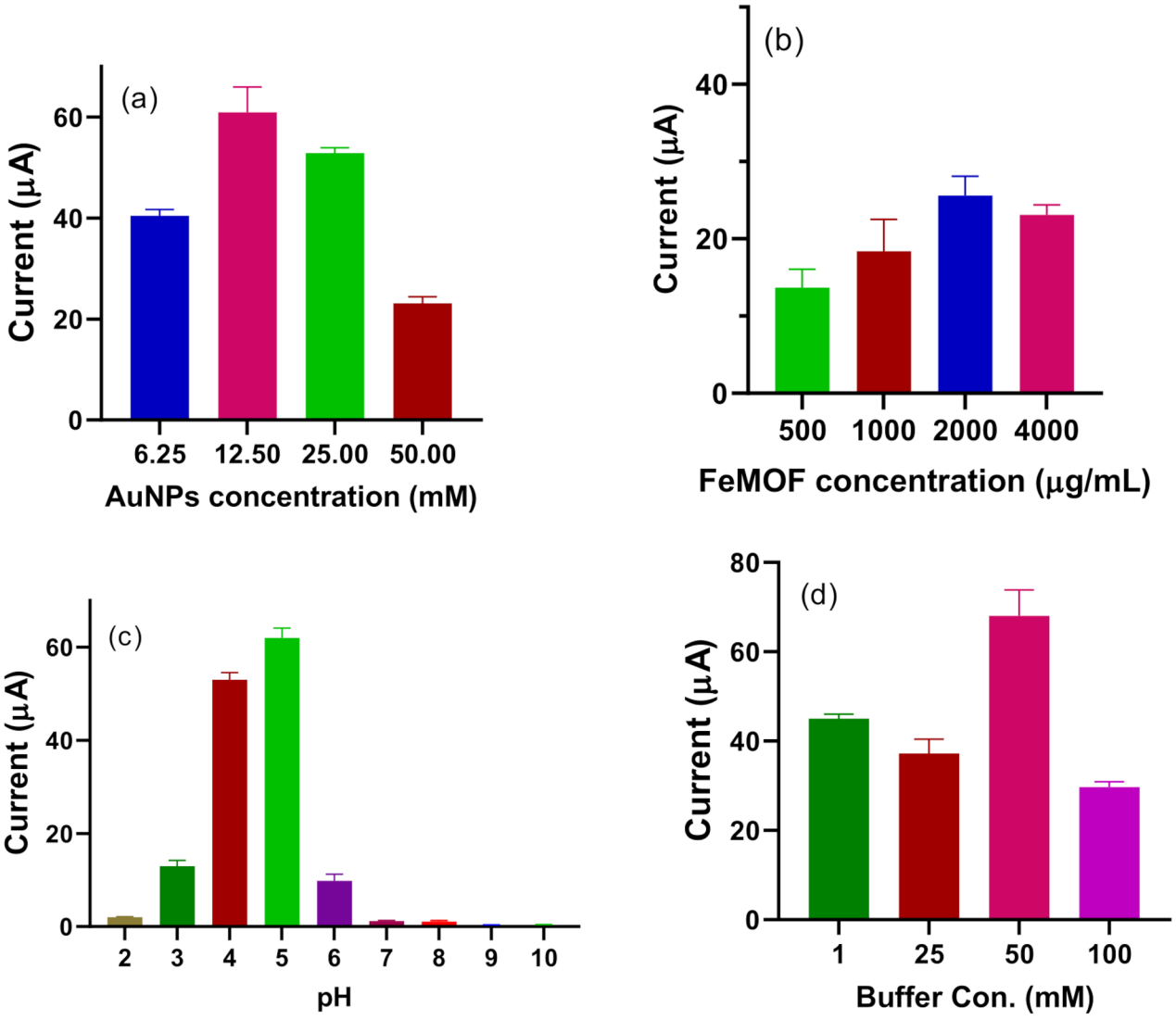

Fig. 4 Optimization of the (**a**) amount of AuNPs, (**b**) FeMOF (µg/mL), (**c**) pH, (**d**) buffer concentration in the fabrication of the probe. ([RIS] 10 µg/mL, pH 5.0, $[Fe(CN)_6]^{-4}/[Fe(CN)_6]^{-3}$, 5 mM, KCl 0.1 M, potential range – 1.0–1.0 V, scan rate 100 mV/s)

relative standard deviation (RSD%) founded to be 3.82-5.96% and 4.35-10.36%, respectively. As shown in Table 2, the mean variations were less than 5%, which is acceptable according to the Food and Drug administration (FDA) ranges for RSD% and RE% (± 15%) for all concentrations, except LLOQs (± 20%).

Specificity of the probe

The specificity of modified GCE was studied in the presence of interfering agents which may disrupt the probe function such as co-prescribed neuroleptics and biological available agents (Fig. 9S). In the presence of a constant concentration of RIS (1 µg/mL), the probe signal was recorded and selective function of the probe determined by RE%. It was observed the performance of the developed method in presence of all interfering agents was influenced less than 20%, except for tryptophan and citric acid.

Stability and effect of biological sample matric

Various types of stability tests are suggested for evaluation of the pharmaceuticals stability in a particular matrix such as freeze-thaw method, short-term temperature stability, stock solution stability, and etc. Freeze-thaw stability was investigated by two concentrations of analyte-spiked samples in three replications. Samples are frozen and thawed in three cycles and then used for stability tests [50]. In addition, stock solution stability was checked by the remaining the prepared standard stocks of analyte for at least 6 h at room temperature [50]. Table 3 lists the measured values, expressed by RE%, which confirms that stability of RIS is independent of

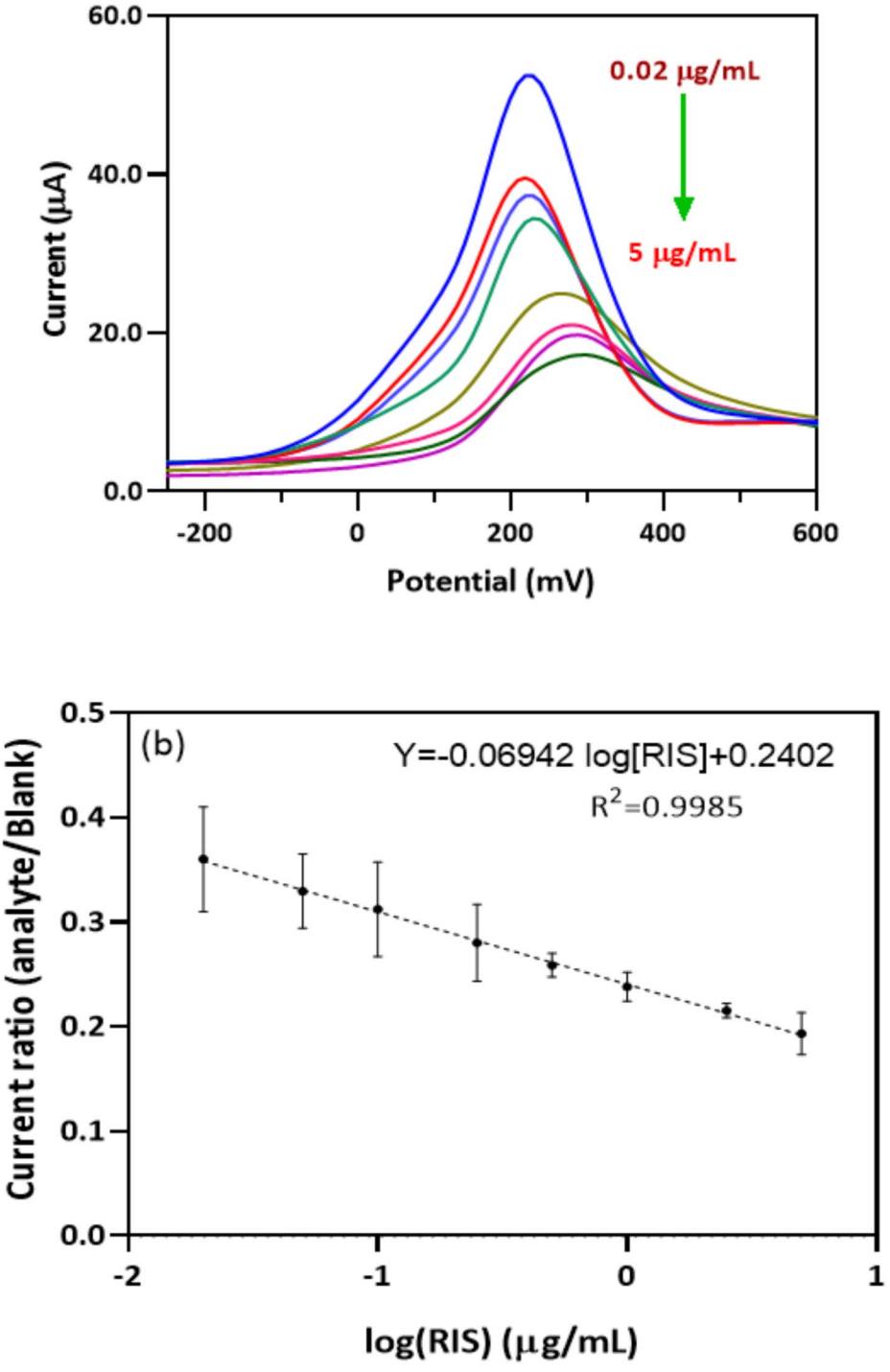

Fig. 5 (**a**) SWVs of FeMOF/AuNPs/GCE probe in the presence of different RIS concentrations and (**b**) calibration curve in plasma media (pH 5.0, $[Fe(CN)_6]^{-4}$/$[Fe(CN)_6]^{-3}$, 5 mM, KCl 0.1 M, scan rate 100 mV/s, pH = 5.0)

sample preparation conditions. Furthermore, the stability of modified GCE was also checked by plotting CVs at different cycle numbers. As the number of CVs increased, the peak current decreased, indicating that the fabricated platform becomes useable after the cycles. The stability of the electrodes was also tested over seven consecutive days. To do this, the electrochemical signal of the electrodes was measured on different days after preparation. The results showed that the intensity of the generated signal did not change significantly until the fourth day.

Table 1 Analytical techniques and performance of the developed methods for RIS quantification

Technique	Samples	Dynamic range (µg/mL)	LOD/LLOQ (µg/mL)	Ref.
Optical (Fluorescence)	Human urine	-	0.103	[1]
Optical (Fluorescence)	Pharmaceutical, human plasma	5–150 ng/mL	1.37 ng/mL	[19]
HPLC-UV	pharmaceutical preparations	10–60	1.79	[44]
UPLC-MS/MS	spiked human serum	0.200–500 ng/mL	LLOQ = 0.2 ng/mL	[45]
Electrochemical (AdSDPV)	Pharmaceutical, spiked human serum	0.04–0.82	0.04	[4]
Electrochemical (SWV)	pharmaceutical preparations	0.02–32.1	0.02	[8]
Electrochemical (SWVs)	Human plasma	0.02-50	LLOQ = 0.02	This work

HPLC: high performance liquid chromatography; UV: ultraviolet, UPLC-MS/MS: ultra-high performance liquid chromatography tandem mass spectrometry; AdSDPV: Adsorptive stripping differential pulse voltammetry; SWV: square-wave voltammetry; LOD: Limit of detection;

Table 2 Repeatability and accuracy of the FeMOF/AuNPs/GCE-based method for RIS detection in unprocessed plasma samples

Added (µg/mL)	Interday			Intraday	
	Obtained (± SD)	Precision (RSD%)	Accuracy (RE%)	Obtained (± SD)	Precision (RSD%)
0.05	0.048 (± 0.0052)	10.78	-4.4	0.051 (± 0.003)	5.96
0.5	0.54 (± 0.024)	4.35	8.9	0.49 (± 0.019)	3.82
5.0	5.19 (± 0.54)	10.36	3.8	4.85 (± 0.26)	5.20

Table 3 Stock solution and freeze-thaw stabilities of the RIS standard solution

Added (µg/mL)	Stock solution		Freeze-thaw	
	found (µg/mL)	Accuracy (RE %)	found (µg/mL)	Accuracy (RE %)
0.5	0.44 (± 0.02)	-12.0	0.48 (± 0.04)	-4.4
5.0	5.12 (± 0.12)	2.4	4.56 (± 0.21)	-8.8

Table 4 Determination of RIS levels in patient plasma samples

No.	M/F	Age (year)	Detected concentration (µg/mL)	HPLC	T-test (*p*-value)
1	F	31	0.0457	0.049	0.78
2	F	35	0.073	0.062	
3	F	46	0.089	0.077	
4	F	40	0.0104	0.023	
5	F	44	0.051	0.145	-*

* This data was excluded

However, after the fifth day, the changes in signal intensity were significant. This indicates that the prepared electrodes are stable in the refrigerator for at least four days (Fig. 10S).

To investigate the effect of the matrix of biological samples, the electrochemical signal was tested in different plasmas. The results showed that the obtained electrochemical peaks did not differ significantly from each other with RSD% less than 10% for recorded signals across all samples (Fig. 11S).

Applications in real samples

In order to evaluate the analytical applicability of the FeMOF/AuNPs modified GCE, five plasma samples were collected from patients with receiving RIS medication regime. Briefly, 1 mL of plasma samples was added to about 4 mL of $[Fe(CN)_6]^{-4}/[Fe(CN)_6]^{-3}$ solution. Despite the previous reported methods, the developed probe used without any protein precipitation and centrifugal separation. The obtained results for the determination of RIS using calibration curve equation in patients' plasma samples are presented in Table 4. The data obtained were compared with an HPLC method previously presented by this group [42]. The results of the t-test indicated no significant difference between the two groups, except for one outlier. When this case was excluded, the *p*-value increased from 0.43 to 0.78. A paired t-test revealed no significant difference between the reported method and HPLC-method (t-value = 0.299, $p = 0.784$, two-tailed). The mean difference was − 0.0018 ± 0.0119 (95% CI: -0.021 to 0.017), with an exceptionally strong pairwise correlation ($r = 0.995$, $p = 0.002$), confirming the robustness of the paired design. This outlier (marked with *) was excluded because the measured concentration (0.051 vs. 0.145 µg/mL) exceeded the 95% prediction interval. Due to sample volume constraints, measurements were performed once per sample, precluding variability assessment. Results should be interpreted as preliminary.

Conclusions

The FeMOF/AuNPs/GCE was fabricated and applied for the study of the electrochemical probe which demonstrated excellent activity for RIS in the presence of $[Fe(CN)_6]^{-4}/[Fe(CN)_6]^{-3}$ redox pair. Despite the bare electrode, the oxidation current of RIS varied negatively by 29 mV by modified electrode. Under optimized condition, the CV responses of the sensor indicates good linearity in the range of 0.02–50 µg/mL with an LLOQ of 0.02 µg/mL. Also, the modified electrode was validated by high accuracy, good repeatability, and long-term stability for the quantitation of RIS. Ultimately, the efficiency of the modified electrode was evaluated by the determination of RIS in patients' plasma samples directly with no need for protein precipitation step prior to the analysis. This newly developed probe shows promise for on-site application without any time–consuming pretreatment steps. The proposed method, with further validation and testing in more real samples, can be used as a reliable method for measuring RIS in clinics. Also, due to its high sensitivity and selectivity, and the use of relatively inexpensive materials in the preparation of the probe, it can be commercially available as a screen-printed electrode for fast and reliable detection of RIS after proper validations.

Supplementary Information

The online version contains supplementary material available at https://doi.org/10.1186/s13065-025-01498-y.

Supplementary Material 1

Acknowledgements
The authors would like to thank the Pharmaceutical Analysis Research Center for its support.

Author contributions
Z.G. and H.P. carried out experiments and wrote the first draft, E.R. and A.J. investigated and reviewed the final version, F.R. provided resources and reviewed first draft, A.F. collected biological samples and reviewed the first draft, J.S. conceptualized the sensing approach, probe fabrication, and validation section, and reviewed the final version.

Funding
This work was supported by the Tabriz University of Medical Sciences (Project Number 71960).

Data availability
Data are available on request from the authors.

Declarations

Ethics approval and consent to participate
This study was conducted in accordance with the principles of the Declaration of Helsinki. Ethical approval was obtained from Research Ethics Committee of Tabriz University of Medical Sciences (Approval No. IR.TBZMED.PHARMACY.REC.1402.015), and informed consent was obtained from all participants. Also, this study complies with all regulations.

Consent for publication
All authors approved the publication of the current study.

Competing interests
The authors declare no competing interests.

Author details
[1]Pharmaceutical Analysis Research Center, Tabriz University of Medical Sciences, Tabriz, Iran
[2]Faculty of Pharmacy, Iran University of Medical Sciences, Tehran, Iran
[3]Faculty of Pharmacy, Tabriz University of Medical Sciences, Tabriz 51666-53431, Iran
[4]Research Center of Psychiatry & Behavioral Sciences, Tabriz University of Medical Sciences, Tabriz, Iran

Received: 6 January 2025 / Accepted: 1 May 2025
Published online: 15 May 2025

References

1. Song J, Luo H, Pan T, Jiang H, Wu Y, Yu X. A new sensitive fluorescence probe based on the molecular recognition for the detection of antipsychotics in human urine. J Photochem Photobiol Chem. 2024;456 January:115807.
2. Saar E, Beyer J, Gerostamoulos D, Drummer OH. The analysis of antipsychotic drugs in human matrices using LC-MS(/MS). Drug Test Anal. 2012;4:376–94.
3. Mandrioli R, Mercolini L, Lateana D, Boncompagni G, Raggi MA. Analysis of risperidone and 9-hydroxyrisperidone in human plasma, urine and saliva by MEPS-LC-UV. J Chromatogr B Anal Technol Biomed Life Sci. 2011;879:167–73.
4. Arvand M, Pourhabib A. Adsorptive stripping differential pulse voltammetric determination of risperidone with a multi-walled carbon nanotube-ionic liquid paste modified glassy carbon electrode. J Chin Chem Soc. 2013;60:63–72.
5. Yatham LN, Grossman F, Augustyns I, Vieta E, Ravindran A. Mood stabilisers plus risperidone or placebo in the treatment of acute mania. Br J Psychiatry. 2003;182:141–7.
6. Stein DJ, Bouwer C, Hawkridge S, Emsley RA. Risperidone augmentation of serotonin reuptake inhibitors in obsessive- compulsive and related disorders. J Clin Psychiatry. 1997;58:119–22.
7. Hirose S, Ashby CR. An open pilot study combining risperidone and a selective serotonin reuptake inhibitor as initial antidepressant therapy. J Clin Psychiatry. 2002;63:733–6.
8. Molaakbari E, Mostafavi A, Tohidiyan Z, Beitollahi H. Synthesis and application of conductive polymeric ionic liquid/ni nanocomposite to construct a nanostructure based electrochemical sensor for determination of risperidone and methylphenidate. J Electroanal Chem. 2017;801:198–205.
9. Ruan CJ, Guo W, Zhou M, Guo GX, Wang CY, Li WB et al. Quantitative determination of risperidone, paliperidone and olanzapine in human serum by liquid chromatography–tandem mass spectrometry coupled with on-line solid-phase extraction. Biomed Chromatogr. 2018;32.
10. Aravagiri M, Marder SR, Wirshing D, Wirshing WC. Plasma concentrations of risperidone and its 9-hydroxy metabolite and their relationship to dose in schizophrenic patients: simultaneous determination by a high performance liquid chromatography with electrochemical detection. Pharmacopsychiatry. 1998;31:102–9.
11. Woestenborghs R, Lorreyne W, Van Rompaey F, Heykants J. Determination of risperidone and 9-hydroxyrisperidone in plasma, urine and animal tissues by high-performance liquid chromatography. J Chromatogr B Biomed Sci Appl. 1992;583:223–30.
12. Olesen OV, Linnet K. Simplified high-performance liquid chromatographic method for determination of risperidone and 9-hydroxyrisperidone in serum from patients comedicated with other psychotropic drugs. J Chromatogr B Biomed Appl. 1997;698:209–16.
13. Le Moing JP, Edouard S, Levron JC. Determination of risperidone and 9-hydroxyrisperidone in human plasma by high-performance liquid chromatography with electrochemical detection. J Chromatogr B Biomed Sci Appl. 1993;614:333–9.
14. Flarakos J, Luo W, Aman M, Svinarov D, Gerber N, Vouros P. Quantification of risperidone and 9-hydroxyrisperidone in plasma and saliva from adult and pediatric patients by liquid chromatography-mass spectrometry. J Chromatogr A. 2004;1026:175–83.
15. Alcantara GKS, Calixto LA, Rocha BA, Júnior FB, de Oliveira ARM, de Gaitani CM. A fast DLLME-LC-MS/MS method for risperidone and its metabolite 9-hydroxyrisperidone determination in plasma samples for therapeutic drug monitoring of patients. Microchem J. 2020;156.

16. Kousoulos C, Dotsikas Y, Loukas YL. Turbulent flow and ternary column-switching on-line clean-up system for high-throughput quantification of risperidone and its main metabolite in plasma by LC-MS/MS. Application to a bioequivalence study. Talanta. 2007;72:360–7.
17. Remmerie BMM, Sips LLA, De Vries R, De Jong J, Schothuis AM, Hooijschuur EWJ, et al. Validated method for the determination of risperidone and 9-hydroxyrisperidone in human plasma by liquid chromatography-tandem mass spectrometry. J Chromatogr B Anal Technol Biomed Life Sci. 2003;783:461–72.
18. Aravagiri M, Marder SR. Simultaneous determination of risperidone and 9-hydroxyrispepidone in plasma by liquid chromatography/electrospray tandem mass spectrometry. J Mass Spectrom. 2000;35:718–24.
19. Alaqel SI, Abdullah O, Alharbi A, Althobaiti YS, Alturki MS, Ramzy S, et al. Guava-fruit based synthesis of carbon quantum dots for spectrofluorometric quantitative analysis of risperidone in spiked human plasma and pharmaceutical dosage forms. RSC Adv. 2023;13:17765–74.
20. Jones T, Van Breda K, Charles B, Dean AJ, McDermott BM, Norris R. Determination of risperidone and 9-hydroxyrisperidone using HPLC, in plasma of children and adolescents with emotional and behavioural disorders. Biomed Chromatogr. 2009;23:929–34.
21. Ko E, Tran VK, Son SE, Hur W, Choi H, Seong GH. Characterization of Au@PtNP/GO nanozyme and its application to electrochemical microfluidic devices for quantification of hydrogen peroxide. Sens Actuators B Chem. 2019;294:166–76.
22. Ribeiro JA, Pereira CM, Silva AF, Sales MGF. Electrochemical detection of cardiac biomarker myoglobin using polyphenol as imprinted polymer receptor. Anal Chim Acta. 2017;981:41–52.
23. Shahrokhian S, Hafezi Kahnamoui M, Salimian R. Surface modification of glassy carbon electrode with the functionalized carbon nanotube for ultrasensitive electrochemical detection of risperidone. J Iran Chem Soc. 2018;15:1485–94.
24. Merli D, Dondi D, Pesavento M, Profumo A. Electrochemistry of olanzapine and risperidone at carbon nanotubes modified gold electrode through classical and DFT approaches. J Electroanal Chem. 2012;683:103–11.
25. Soleymani J, Azizi S, Abbaspour-Ravasjani S, Hasanzadeh M, Somi MH, Jouyban A. Glycoprotein-based bioimaging of HeLa cancer cells by folate receptor and folate decorated graphene quantum dots. Microchem J. 2021;170:106732.
26. Hasanzadeh M, Rahimi S, Solhi E, Mokhtarzadeh A, Shadjou N, Soleymani J, et al. Probing the antigen-antibody interaction towards ultrasensitive recognition of cancer biomarker in adenocarcinoma cell lysates using layer-by-layer assembled silver nano-cubics with porous structure on cysteamine caped GQDs. Microchem J. 2018;143:379–93.
27. Bagheri M, Masoomi MY. Sensitive ratiometric fluorescent metal-organic framework sensor for calcium signaling in human blood ionic concentration media. ACS Appl Mater Interfaces. 2020;12:4625–31.
28. Hu Z, Deibert BJ, Li J. Luminescent metal-organic frameworks for chemical sensing and explosive detection. Chem Soc Rev. 2014;43:5815–40.
29. Monguzzi A, Ballabio M, Yanai N, Kimizuka N, Fazzi D, Campione M, et al. Highly fluorescent metal-organic-framework nanocomposites for photonic applications. Nano Lett. 2018;18:528–34.
30. Furukawa H, Cordova KE, O'Keeffe M, Yaghi OM. The chemistry and applications of metal-organic frameworks. Sci (80-). 2013;341:1230444.
31. Dykman L, Khlebtsov B, Khlebtsov N. Drug delivery using gold nanoparticles. Adv Drug Deliv Rev. 2025;216:115481.
32. Shamloo HB, Jafarzadeh S, Jouyban A, Soleymani J. Synthesis and application of concanavalin A-conjugated green luminescent gold nanoparticle/fluorescent polydopamine nanoparticles for specific differentiation of cancer cells from normal cells using glycan bioreceptors. Mater Chem Phys. 2022;288:126344.
33. Zare Y, Maghsoudi-Salek M, Golsanmalou Z, Jouyban AJS, Bagherpour-Shamloo H. Synthesis and characterization of folate-functionalized silica-based smart materials and application for bioimaging of cancer cells. Heliyon. 2022;:Revised.
34. Soleymani J, Hasanzadeh M, Somi MH, Jouyban A. Differentiation and targeting of HT 29 cancer cells based on folate bioreceptor using cysteamine functionalized gold nano-leaf. Mater Sci Eng C. 2020;107:110320.
35. Hasanzadeh M, Solhi E, Jafari M, Mokhtarzadeh A, Soleymani J, Jouyban A, et al. Ultrasensitive immunoassay of tumor protein CA 15.3 in MCF-7 breast cancer cell lysates and unprocessed human plasma using gold nanoparticles doped on the structure of mesoporous silica. Int J Biol Macromol. 2018;120:2493–508.
36. Sintya V, Saefumillah A, Zulys A. Development study of iron-based metal organic frameworks (Fe-based MOFs) as a binding agent in diffusive gradient in thin film method (DGT) for phosphate adsorption. IOP Conf Ser Mater Sci Eng. 2020;902:12026.
37. Chaichi MJ, Ehsani M. A novel glucose sensor based on immobilization of glucose oxidase on the chitosan-coated Fe3O4 nanoparticles and the luminol-H2O2-gold nanoparticle chemiluminescence detection system. Sens Actuators B Chem. 2016;223:713–22.
38. Hezard T, Fajerwerg K, Evrard D, Collière V, Behra P, Gros P. Influence of the gold nanoparticles electrodeposition method on Hg(II) trace electrochemical detection. Electrochim Acta. 2012;73:15–22.
39. Zhang Y, Zhang D, He Y, Wang Z, Song P, Wang R. Construction of hexagonal spindle-shaped Fe-MOFs induced by cationic copolymer and its application for effective wastewater treatment. Environ Sci Pollut Res. 2023;30:80279–92.
40. Paiman SH, Rahman MA, Uchikoshi T, Abdullah N, Othman MHD, Jaafar J, et al. Functionalization effect of Fe-type MOF for methylene blue adsorption. J Saudi Chem Soc. 2020;24:896–905.
41. Rahmani E, Rahmani M. Alkylation of benzene over Fe-based metal organic frameworks (MOFs) at low temperature condition. Microporous Mesoporous Mater. 2017;249:118–27.
42. Feyzi F, Soleymani J, Dastmalchi S, Ranjbar F, Jouyban A. Dispersive solid-phase extraction of risperidone from plasma samples using graphene oxide aerogels and determination with liquid chromatography. J Sep Sci. 2023;46:2201028.
43. Bhandari V, Singh H. Analytical methods: physical methods. 2002.
44. Dedania ZR, Dedania RR, Sheth NR, Patel JB, Patel B. Stability indicating HPLC determination of risperidone in bulk drug and pharmaceutical formulations. Int J Anal Chem. 2011;2011:1–6.
45. Ezzeldin E, Tammam M, Abo Talib NF. New modified UPLC/Tandem mass spectrometry method for determination of risperidone and its active metabolite 9-hydroxyrisperidone in plasma: application to dose-dependent pharmacokinetic study in Sprague-Dawley rats. Int J Anal Chem. 2017;2017:1271383.
46. Park SH, Kwon N, Lee JH, Yoon J, Shin I. Synthetic ratiometric fluorescent probes for detection of ions. Chem Soc Rev. 2020;49:143–79.
47. Soleymani J, Perez-Guaita D, Hasanzadeh M, Shadjou N, Jouyban A. Materials and methods of signal enhancement for spectroscopic whole blood analysis: novel research overview. TrAC Trends Anal Chem. 2017;86:122–42.
48. Soleymani J, Hasanzadeh M, Eskandani M, Khoubnasabjafari M, Shadjou N, Jouyban A. Electrochemical sensing of doxorubicin in unprocessed whole blood, cell lysate, and human plasma samples using thin film of poly-arginine modified glassy carbon electrode. Mater Sci Eng C. 2017;77:790–802.
49. Hasanzadeh M, Shadjou N. Electrochemical nanobiosensing in whole blood: recent advances. TrAC - Trends Anal Chem. 2016;80:167–76.
50. Zhang Z, Hao J, Zhang J, Zhang B, Tang J. Protein as the source for synthesizing fluorescent carbon dots by a one-pot hydrothermal route. RSC Adv. 2012;2:8599–601.

Publisher's note